

Quantitative analysis of bonding in 90° partial dislocation in diamond

This article has been downloaded from IOPscience. Please scroll down to see the full text article.

2000 J. Phys.: Condens. Matter 12 10325

(<http://iopscience.iop.org/0953-8984/12/49/336>)

View [the table of contents for this issue](#), or go to the [journal homepage](#) for more

Download details:

IP Address: 171.66.16.226

The article was downloaded on 16/05/2010 at 08:12

Please note that [terms and conditions apply](#).

Quantitative analysis of bonding in 90° partial dislocation in diamond

S Jenkins and M I Heggie

CPES, University of Sussex, Falmer, Brighton BN1 9QJ, UK

Received 28 September 2000

Abstract. The soliton model for motion of the 90° partial in silicon has provided an explanation for the large reduction in activation energy (1 eV) which occurs under prolonged exposure to an H plasma. Applying the same theoretical model to diamond yields a drop of 1.6 eV and puts dislocation motion into the realm of the possible. Here we examine with the ‘atoms in molecules’ method the bonding in the local energy minima and saddle point structures involved in motion of the 90° partial. We find bonds with graphite character in the soliton, and, to a greater extent, in its saddle points for motion and kink pair nucleation. The presence of H does not suppress this character in any structure other than the kink pair, in which H is far less compressed. Furthermore we characterize the over-coordination of H in these structures.

1. Introduction

Chemistry was revolutionized by the concept of valence, which subsequently found a natural explanation in quantum mechanics. Adjectives to describe bonding, such as electronegative, covalent, ionic, metallic, covalent and hybridized, have been of enormous utility in research and teaching. The imprecision of these terms (even for ground state systems) is well known, but they are severely stretched when applied to more energetic systems, such as point and extended defects in semiconductors. For example, in this paper we are concerned with diamond, in which the Frenkel pair energy is of the order of 20 eV [1] and we shall be studying saddle points ~ 2 eV above neighbouring minima.

The problem to be confronted is that the full, dynamical quantum mechanical simulation for electrons in a system large enough to reproduce properties of dislocations and run for long enough to reliably illustrate rare events such as kink pair nucleation and impurity pinning is not yet possible. In a different area, it was shown that such an approach was not yet practical in trying to reproduce the observation that the growth process of the C₆₀ molecule always yields the unique I_h symmetry isomer. An alternative approach was necessary: enumeration of all possible isomers and pathways between them, then structural optimization and vibrational analysis of each isomer and application of the energy landscape method to follow the annealing [2]. Such an enumeration was possible through the topological rules which govern bonding in fullerene structures.

In the case of dislocations, especially interacting with impurities, it has been necessary to understand bonding, and how it changes, in order to select, at the least, reasonable starting structures for simulations, static optimizations or saddle point location algorithms. With this purpose, we use the ‘atoms in molecules’ (AIM) method [3] to describe bonding from an analysis of the charge density (in our case resulting from a first principles calculation, but

it is possible to start from experiment). Our objective in using AIM is to understand weak and strained bonds, and, in particular, bonds which lie outside the range of normal chemical descriptions. It should be emphasized that total energy is in general a property of the whole system, but we investigate the extent to which two body and local descriptions are valid.

2. Method

2.1. First principles calculations

All geometries and energies for minima and saddle points on the energy surface were calculated with AIMPRO [4] as reported elsewhere in this volume [5]. These calculations parallel those in silicon [6] and involve the classical trajectories and energy surfaces. The topological study of charge density was performed on smaller clusters (typically $C_{52}H_{52}$) including the core of the defect cut from the larger AIMPRO cluster. The C–C bonds cut to produce the smaller cluster were replaced with C–H bonds of length 1.0 Å following the original bond direction.

The total charge density distributions for the smaller cluster were obtained using CRYSTAL98 [7], where 6-21G basis sets were used throughout. The charge densities for energy minima were obtained with DFT (generalized gradient approximation of Perdew and Wang [8]) and for saddle point structures with unrestricted Hartree Fock method (UHF), where convergences of the energy and eigenvalues were 10^{-5} and 10^{-6} au, respectively, in all cases. Test calculations proved the AIM derived quantities to be insensitive to choice of basis set. Analyses of the electron density and the determination of the atomic properties were performed using TOPOND98 [9].

In the AIMPRO study [5], the soliton model for dislocation motion was studied in both the presence and absence of H. This model exploits the reactivity of the dangling bond associated with the soliton (figure 1(a) illustrates the soliton bound to an H atom) and the topological properties of the reconstruction bonds. For economy of space we depict, in figure 1, glide plane diagrams of the core of the soliton and its saddle points for motion when it is bonded to H, but the diagrams omitting H apply also to the non-hydrogenated case (albeit with small changes in geometry). These structures are discussed in detail in section 3, but first we discuss the AIM method.

2.2. Atoms in molecules

The charge density $\rho(\mathbf{r})$ is a scalar field and its topological properties are reducible to a description of the number and type of its *critical points* (where $\nabla\rho(\mathbf{r}_{critical}) = 0$). These extrema in $\rho(\mathbf{r})$ can be characterized by the (3×3) matrix of second partial derivatives with respect to coordinates of the charge density (the *Hessian* matrix), which, when diagonalized, has four possible signatures (m, n) , expressed as the number, m , of non-zero eigenvalues, and the arithmetic sum, n , of the signs of the eigenvalues (± 1). Of relevance to our work are the bond critical point or BCP $(3, -1)$, the ring critical point or RCP $(3, +1)$ and the cage critical point or CCP $(3, +3)$.

At a BCP, two curvatures are negative and ρ is a maximum at $\mathbf{r}_{critical}$ in the plane defined by their corresponding axes. ρ is a minimum at $\mathbf{r}_{critical}$ along the third axis, perpendicular to this plane. It is a necessary condition for the formation of a bound state and it implies the existence of an atomic interaction line—a line linking the nuclei along which the charge density is a maximum with respect to any neighbouring line. If the forces resulting from the accumulation of electronic charge in the binding region are sufficient to exceed the anti-binding forces over a range of separations to yield an equilibrium configuration, then the state is bound

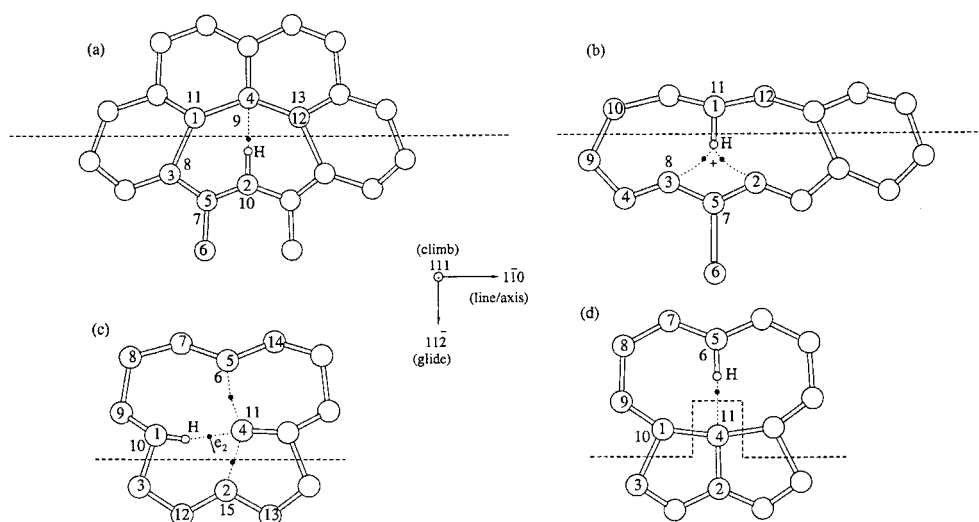


Figure 1. Glide plane diagrams of the core of a soliton on a 90° partial in diamond and the saddle points, metastable states and products of its motion. All structures are for the case when H is present, but when interacting with H. (a) Soliton. (b) Saddle point to motion along core. (c) Metastable state during kink pair nucleation. (d) Kink pair nucleated at soliton. Numbers are as referred to in tables 2–8 inclusive. The plane of the diagram is (111), left/right is (1 – 10) and up is $\langle 11 - 2 \rangle$. The dislocation axis is shown as a broken line.

and the atomic interaction line is called a *bond path*. The molecular graph isolates the pairwise interactions present in a group of atoms which dominate and characterize the properties of the system whether it is at equilibrium or in a state of change. The bond critical points (BCPs) are found to join some (but not all) of the pairs of nuclei in a molecule.

At an RCP two curvatures are positive and ρ is a minimum in the plane defined by their corresponding axes. ρ is a maximum along the third axis, perpendicular to this plane. At a CCP all curvatures are positive and ρ is a local minimum.

Critical points may further be characterized by the (rotationally invariant) Laplacian of $\rho(\mathbf{r})$, $\nabla^2\rho$, and by the principal axes and corresponding curvatures from the eigenvectors and corresponding ordered eigenvalues ($\lambda_1 < \lambda_2 < \lambda_3$) in the diagonalization of the Hessian of $\rho(\mathbf{r}_b)$. Using AIM all interactions are categorized as one of two types, where there is a continuum of chemical character in between. These two types of interaction are designated according to the sign of the Laplacian of the charge density at the BCP, $\nabla^2\rho(\mathbf{r}_b)$: it is positive for a ‘closed shell’ and negative for a ‘shared shell’ interaction. Examples of the former type of interaction include the strong ‘covalent’ carbon–carbon bonds in diamond, and those of the latter type include hydrogen bonds. Relatively recently anion–anion bonding interactions [10–12] have been quantified within AIM.

The ellipticity denoted by $\varepsilon = \lambda_1/\lambda_2 - 1$ provides a measure of the extent to which charge is preferentially accumulated in a given plane. It indicates π character as well as bond instability [13] and has previously [14] been linked to the plane in which atoms most easily slide. As the separation between a BCP and an RCP (or D_{br}), decreases, the ellipticity, ε , increases until it tends to infinity when the points coalesce and the bond path is then ruptured.

A degree of covalent character can be assigned [15] to a bond for negative values of $H(\mathbf{r}_b)$, the total local energy density. All bonds investigated in this article satisfy this condition. The dissociation energy per bond, D_e , can be obtained from the atomic virial theorem [16, 17],

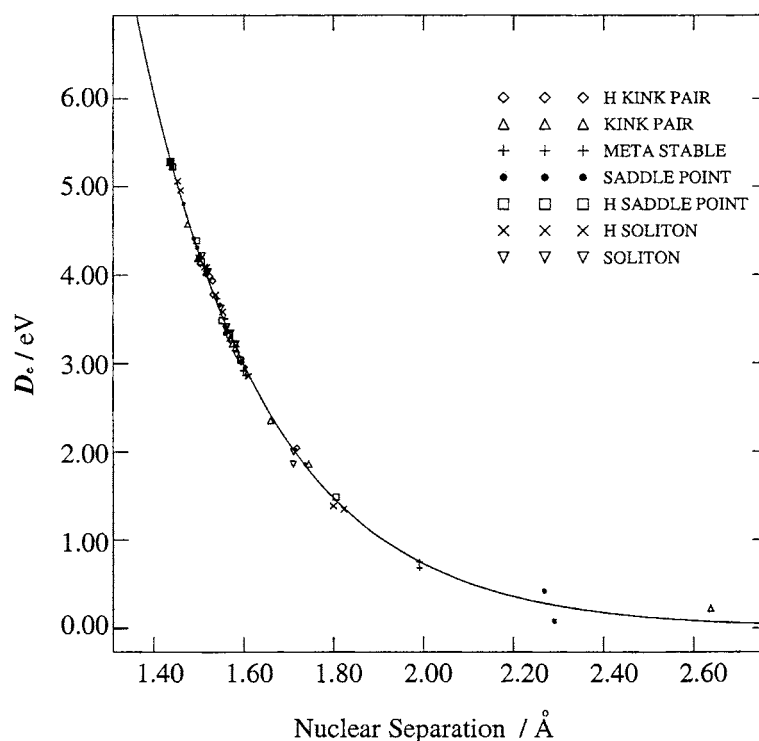


Figure 2. Dissociation energy (D_e) dependence on C–C internuclear separations, $d(\text{C–C})$, for both shared shell and closed shell bonding interactions. The solid line corresponds to the exponential fitting: $D_e = A \exp[-Bd(\text{C–C})]$, with $A = 843 \text{ eV}$, $B = 3.53 \text{ \AA}^{-1}$.

and all D_e values reported in this paper were found to depend exponentially on internuclear separations (figure 2) according to

$$D_e = A \exp[-Bd]$$

with $A = 843 \text{ eV}$, $B = 3.53 \text{ \AA}^{-1}$ and d the C–C internuclear distance.

This is not a simple two-body interaction as would be written in a simple interatomic potential; it is a relationship which holds for structures in mechanical equilibrium and only applies to two-body interactions when there is a BCP between the bodies. This latter criterion is many-body and quantum mechanical in nature. The fit is remarkable, with only a small departure at large $d(\text{C–C})$.

3. Results and discussion

The data are presented in tables 1–8, where $d(\text{C–X})$ is the nuclear separation ($X = \text{H or C}$).

Table 1 contains reference DFT calculations for graphite and diamond as both crystals and hydrogenated clusters, with comparators from experimental charge densities. Whereas the $\text{C}_{62}\text{H}_{20}$ graphite cluster appears to be a good representation of the crystal, the smaller $\text{C}_{22}\text{H}_{35}$ diamond cluster is clearly worse.

The BCPs in diamond have zero ellipticity while in graphite it is 0.11 and the λ_2 axis is along $\langle 0001 \rangle$. However, a high value of ε ($\varepsilon > 0.01$) for a weak bond indicates propensity to rupture, rather than π bonding, as found later for reconstruction bonds ($0.08 < \varepsilon < 0.2$).

Table 1. Reference AIM properties for diamond and graphite.

Interaction	$d(\text{C-X})$ (Å)	D_{br} (Å)	$\rho(r_b)$ (au)	$\nabla^2\rho(r_b)$ (au)	ε	$H(r_b)$ (eV)	D_e (eV)
Crystalline graphite							
C-C	1.4190	1.2276	0.2831	-22.7073	0.1068	-8.2683	5.4299
Finite graphite sheet ^a							
C-C	1.4099	1.2274	0.2850	-23.1302	0.1064	-8.3794	5.4870
Crystalline diamond ^b							
C-C	1.5588	1.2730	0.2230	-15.021	0.0000	-5.3856	3.5090
			<i>0.2365</i>	<i>-14.041</i>	<i>0.0000</i>		
Diamond cluster ^c							
C-C	1.5444	1.2735	0.2407	-17.2481	0.0049	-5.9938	3.8378
C-C	1.5554	1.2710	0.2571	-16.7580	0.0000	-6.0214	3.9267
C-C	1.5587	1.2695	0.2365	-16.5395	0.0014	-5.7920	3.7252

^a Single graphite layer consisting of 62 C atoms passivated by 20 H atoms.

^b Figures in italics represent data obtained from experiment [18]; exact correspondence was obtained for $\nabla^2\rho(r_{CCP})$ and $\nabla^2\rho(r_{RCP})$ where the values were 1.769 and 2.45 eV, respectively.

^c Diamond cluster including the (111) plane consisting of 22 C atoms passivated by 35 H atoms: the three values given represent the range of values.

Table 2. AIM properties of the soliton on a 90° partial in diamond (figure 1(a) omitting H).

Inter-action	$d(\text{C-X})$ (Å)	D_{br} (Å)	$\rho(r_b)$ (au)	$\nabla^2\rho(r_b)$ (au)	ε	D_e (eV)
C1-C3	1.71	1.03	0.166	-6.03	0.02	2.00
C1-C4	1.71	1.15	0.162	-6.10	0.01	1.86
C3-C8	1.58	1.07	0.213	-12.55	0.02	3.22
C2-C10	1.56	1.25	0.218	-13.11	0.04	3.42
C1-C11	1.57	0.49	0.219	-13.56	0.02	3.35
C4-C9	1.56	1.33	0.219	-13.84	0.02	3.39
C3-C5	1.52	1.19	0.241	-16.59	0.02	4.04
C2-C5	1.51	1.19	0.246	-17.24	0.03	4.22
C12-C13	1.57	0.52	0.219	-13.53	0.02	3.33

Table 3. AIM properties of the soliton migration saddle point (figure 1(b) omitting H).

Inter-action	$d(\text{C-X})$ (Å)	D_{br} (Å)	$\rho(r_b)$ (au)	$\nabla^2\rho(r_b)$ (au)	ε	D_e (eV)
C1-C2	2.27	0.65	0.053	2.66	0.14	0.42
C1-C3	2.27	0.68	0.056	2.29	0.07	0.43
C1-C12	1.56	1.24	0.218	-13.57	0.02	3.34
C3-C8	1.50	1.27	0.249	-17.62	0.03	4.31
C1-C11	1.49	1.18	0.253	-18.59	0.04	4.41
C4-C3	1.47	1.21	0.266	-20.37	0.02	4.81
C2-C5	1.44	1.09	0.282	-23.20	0.02	5.28
C3-C5	1.44	1.18	0.280	-22.69	0.02	5.23

Also note that the separation between a BCP and an RCP, i.e. D_{br} , in general decreases as a bond path gets closer to rupturing, but it can be seen from table 1 that the stronger, graphite bond has a smaller D_{br} than diamond.

Table 4. AIM properties of a kink pair nucleated at a soliton (figure 1(d), omitting H).

Inter-action	$d(\text{C-X})$ (Å)	D_{br} (Å)	$\rho(r_b)$ (au)	$\nabla^2\rho(r_b)$ (au)	ε	D_e (eV)
C4-C2	1.58	1.07	0.214	-12.84	0.01	3.22
C5-C6	1.48	1.28	0.258	-19.49	0.05	4.58
C5-C7	1.50	1.24	0.245	-17.53	0.05	4.19
C9-C1	1.50	1.28	0.247	-17.99	0.01	4.20
C1-C10	1.52	1.08	0.243	-16.94	0.02	4.08
C4-C11	1.57	1.34	0.214	-12.84	0.01	3.22
C1-C3	1.74	0.99	0.159	-5.30	0.02	1.86
C1-C4	1.66	1.08	0.179	-7.83	0.03	2.35
C4-C5	2.64	1.02	0.026	1.73	0.15	0.22

Table 5. AIM properties of hydrogenated soliton (figure 1(a)).

Inter-action	$d(\text{C-X})$ (Å)	D_{br} (Å)	$\rho(r_b)$ (au)	$\nabla^2\rho(r_b)$ (au)	ε	D_e (eV)
C1-C3	1.82	0.97	0.135	-2.64	0.01	1.34
C1-C4	1.80	1.27	0.141	-3.65	0.01	1.38
C4-H	1.64	0.97	0.065	4.54	0.81	1.07
C3-C8	1.55	1.25	0.226	-14.32	0.01	3.58
C2-C10	1.54	1.24	0.230	-15.14	0.01	3.77
C1-C11	1.51	1.09	0.244	-17.28	0.02	4.09
C4-C9	1.50	1.32	0.246	-17.74	0.02	4.20
C3-C5	1.46	1.18	0.271	-21.19	0.00	4.96
C2-C5	1.45	1.14	0.273	-21.58	0.02	5.06
C2-H	1.04	1.01	0.311	-26.40	0.01	5.38
C1-C12	1.51	1.09	0.244	-17.30	0.02	4.09

Table 6. AIM properties of saddle point for hydrogenated soliton migration (figure 1(b)).

Inter-action	$d(\text{C-X})$ (Å)	D_{br} (Å)	$\rho(r_b)$ (au)	$\nabla^2\rho(r_b)$ (au)	ε	D_e (eV)
C2-H	1.68	0.53	0.072	4.40	0.82	1.14
C3-H	1.68	0.53	0.072	4.41	0.79	1.14
C1-C4	1.55	1.26	0.225	-14.95	0.01	3.49
C3-C8	1.50	1.26	0.252	-18.45	0.06	4.39
C1-C11	1.51	1.25	0.246	-18.15	0.03	4.15
C4-C3	1.44	1.21	0.283	-23.25	0.05	5.28
C3-C5	1.44	0.97	0.280	-22.31	0.07	5.29
C2-C5	1.44	0.97	0.278	-21.93	0.08	5.23
C1-H	1.06	1.14	0.281	-22.04	0.00	4.62

D_e of 5.43 eV for graphite bonds and 3.51 eV for diamond gives approximate values for cohesive energies of 8.15 eV and 7.02 eV, respectively, artificially stabilizing graphite with respect to diamond, but of correct magnitude to within $\sim 10\%$. Agreement is remarkable considering there is no reference calculation made for the atomic carbon. This may mean that D_e values can be summed for the core of the defects to obtain the local energy changes, but the proximity of the surface to our clusters frustrates this exercise.

Table 7. The metastable structure (intermediate in nucleation of kink pair from hydrogenated soliton, figure 1(c)).

Inter- action	$d(\text{C-X})$ (Å)	D_{br} (Å)	$\rho(r_b)$ (au)	$\nabla^2\rho(r_b)$ (au)	ε	D_e (eV)
C4-H	1.60	1.11	0.073	3.94	0.11	1.14
C4-C2	1.99	0.96	0.100	0.15	0.02	0.75
C4-C5	1.99	1.12	0.099	0.03	0.01	0.68
C5-C6	1.50	1.31	0.248	-18.14	0.02	4.21
C5-C7	1.60	1.25	0.203	-11.48	0.01	2.92
C9-C1	1.43	1.30	0.282	-23.25	0.02	5.32
C1-C10	1.56	1.04	0.222	-13.94	0.02	3.50
C4-C11	1.52	1.22	0.241	-16.60	0.02	4.01
C1-C3	1.54	1.00	0.230	-15.15	0.02	3.73
C1-H	1.04	0.97	0.301	-24.73	0.01	5.05
C1-C12	1.48	1.12	0.257	-18.92	0.01	4.53
C2-C12	1.47	1.06	0.263	-20.28	0.02	4.67
C2-C15	1.52	1.28	0.243	-17.26	0.01	4.04

Table 8. AIM properties of the kink pair nucleated at a hydrogenated soliton (figure 1(d)).

Inter- action	$d(\text{C-X})$ (Å)	D_{br} (Å)	$\rho(r_b)$ (au)	$\nabla^2\rho(r_b)$ (au)	ε	D_e (eV)
C4-H	1.67	1.23	0.061	4.04	0.05	0.97
C4-C2	1.53	1.07	0.236	-15.76	0.02	3.93
C5-C6	1.52	1.29	0.241	-17.02	0.02	4.02
C5-C7	1.53	1.25	0.233	-15.84	0.02	3.78
C9-C1	1.50	1.30	0.245	-17.62	0.01	4.13
C1-C10	1.52	1.07	0.240	-16.43	0.02	3.99
C4-C11	1.59	1.35	0.207	-11.68	0.01	3.05
C1-C3	1.72	1.00	0.168	-6.30	0.02	2.04
C5-H	1.05	1.18	0.294	-23.83	0.00	4.82
C1-C4	1.68	1.05	0.175	-7.18	0.02	2.25

Now we turn to the results for the two cases of soliton motion, firstly, in the absence and, secondly, in the presence, of H.

3.1. Diamond without H

With reference to figure 1, but ignoring the H, we report on the bonding of glide plane atoms and those (atom numbers marked outside the circles) connected by $\langle 111 \rangle$ bonds in the climb direction. We preserve the numbering of the clusters used, which differs in 1(c) and 1(d) from that in 1(a) and 1(b). Where symmetries are apparent in these diagrams it is only approximate, being broken by neighbouring glide planes and in some cases by the shape of the cluster surface.

In the soliton (table 2) we note that all interactions are ‘shared shell’ and there are no ‘closed-shell’ interactions on the dangling bond atom, C2. Where such interactions might have been expected (amongst atoms C2, C1, C12), there is instead an RCP (on the line C2-C4). On the basis of their enhanced D_e values, there is evidence that the glide plane ‘back’ bonds to C2 (e.g. C2-C5) have graphitic character. The reconstruction bond is weak ($D_e = 2.0$ eV), but so are the bonds opposite C2 (e.g. C1-C4, $D_e = 1.9$ eV). It is curious that the bonds in the climb

direction (C2–C10, C1–C11 and C12–C13), while strong, have large ellipticities and the latter two have small values of D_{br} , which may signal a previously unnoticed reactivity.

The soliton moves along the dislocation axis with ease (activation energy = 0.30 eV) [5]. The AIM features of the saddle point (table 3) indicate that, although a reconstruction bond C1–C3 of 2 eV has been broken, there are compensations due to increased bond strength (graphite character) in C2–C5, C3–C5, C3–C4 in the glide plane and C3–C8, C1–C11 out of it. Furthermore, weak, 'closed-shell' interactions (of $D_e = 0.42$ eV) appear across the dislocation core (C1–C2 and C1–C3). There is an RCP midway between these two BCPs, so the bond path will easily switch between atoms C2 and C3.

The soliton can nucleate a kink pair as in figure 1(d) (without H). It does so through an activation barrier of 0.74 eV, which we have not yet investigated. The product kink pair is 0.23 eV higher in energy [5], and there are small changes in graphitic nature plus a 'closed-shell' interaction C4–C5 of 0.22 eV (table 4).

3.2. Diamond with H

The origin of the strong bonding of H to the soliton (table 5) lies in the C2–H bond ($D_e = 5.4$ eV). However, the effect appears not to be straightforward saturation (combining soliton with an H atom from the gas phase is exothermic by 2.0 eV [5]). The H atom introduces an extra 'closed-shell' interaction with C4 (1.1 eV). This has a high ε (0.81), indicative of instability, and the presence of H also destabilizes by ~ 0.5 eV the opposing C–C bonds (C1–C3 and C1–C4) and the reconstruction bond (C1–C3). These are signs that the H is in a compressed environment and it may be this compression which preserves the graphitic (high D_e) character of the back bonds and their neighbours, as was seen in the soliton.

The C–H bond in the saddle point for migration (table 6) is weakened by 0.7 eV and the H atom takes part in two closed-shell interactions (with C2 and C3) of $D_e = 1.1$ eV each, which could be described as a bifurcated hydrogen bond [13]. There is evidence for more extensive graphitic nature in the back bonds in this structure compared with the soliton, as was the case when H was absent. It is interesting to speculate that either of these features could contribute to reduction of the barrier to motion below that expected [5] from the barrier in Si. The instability of the saddle point (figure 1(b)) is anticipated from the proximity of the RCP (marked by a cross) to the neighbouring BCPs (dots).

Turning to the nucleation of a kink pair at a hydrogenated soliton, this was found to proceed through the metastable state of figure 1(c), resulting in the kink pair of figure 1(d). The preference of the H to move in the glide plane is indicated (in figure 1(c)) by e_2 , the direction of the λ_2 eigenvalue. This structure was first attempted because it maximized bonding in a 'ball-and-spring' sense. This is verified by AIM, although what were imagined to be strong bonds (C2–C4 and C4–C5) are shown to be modest, closed-shell interactions of $D_e = 0.7$ eV (table 7). The angle strain in these bonds is manifested by the curvature of their bond paths (fine dotted lines, figure 1(c)). The H bond (C4–H) is slightly strengthened at 1.1 eV but it still 'closed shell' and its ellipticity is increased. The shared shell bond C1–H is weaker than in the soliton by 0.3 eV.

Compared with the metastable state, the product kink pair (table 8) of figure 1(d) has a longer, weaker (1.0 eV) H bond (C4–H), but its ellipticity is halved. The C1–C4 bond opposing H is weak (2.2 eV), but not as weak as equivalents in the metastable structure (C2–C4 and C4–C5, $D_e = 0.7$ eV) nor indeed as weak as in the soliton (C1–C4, $D_e = 1.4$ eV). The back bonds C7–C5 and C7–C8 are no longer graphitic in nature, reflecting the less compressed nature of H in this product. Thus the atomic arrangement of the kink pair affords the H atom greater space and explains its negative energy of formation [5] (–0.5 eV) when H is present.

4. Conclusion

In the complex situation here AIM offers a language to describe the evolution of bonding during dislocation motion and it gives insight beyond the 'ball-and-spring' language of 'strained and dangling' bonds. It was not possible to use D_e values to fully 'deconstruct' the DFT total energies: our AIM clusters were too small and there were strong, mutually compensating variations of D_e values between clusters.

It was not surprising that a 'dangling bond' in diamond can give rise to graphitic behaviour in neighbouring bonds, but AIM showed that, where the dangling bond is saturated with H, the behaviour was not suppressed in every case. The only example of suppression of graphitic behaviour was in the kink pair, where H is not in a compressed environment (and this probably explains why kink pair formation, while not spontaneous, is thermodynamically favoured in the presence of H).

Acknowledgments

We thank Chris Ewels, Nic Harrison (re CRYSTAL98) and Carlo Gatti (re TOPOND98) for helpful discussions and provision of data and software. We acknowledge the Transdiam project of the EU program Interreg II for financial support, and the Sussex High Performance Computing Initiative for computing support.

References

- [1] Breuer S and Briddon P R 1995 *Phys. Rev. B* **51** 6984
- [2] Walsh T R and Wales D J 1998 *J. Chem. Phys.* **109** 6691
- [3] Bader R F W 1998 *Atoms in Molecules: a Quantum Theory (The International Series of Monographs on Chemistry 22)* (Oxford: Oxford University Press)
- [4] Jones R and Briddon P R 1998 *Semicond. Semimet.* A **51** 287
- [5] Heggie M I, Jenkins S, Ewels C P, Briddon P R and Jones R 2000 *J. Phys.: Condens. Matter* at press
- [6] Ewels C P, Leoni S, Heggie M I, Jemmer P and Hernández E 2000 *Phys. Rev. Lett.* **82** 690
- [7] Saunders V R, Dovesi R, Roetti C, Causà M, Harrison N M, Orlando R and Zicovich-Wilson C M 1998 *CRYSTAL98 User's Manual* University of Torino
- [8] Perdew J P and Wang Y 1986 *Phys. Rev. B* **33** 8800
Perdew J P and Wang Y 1989 *Phys. Rev. B* **40** 3399
Perdew J P and Wang Y 1992 *Phys. Rev. B* **45** 13 244
- [9] Gatti C 1999 *TOPOND 98 User's Manual* CNR-CSR SRC Milano
- [10] Pendás A M, Costales A and Luaña V 1997 *Phys. Rev. B* **55** 4275
- [11] Luaña V, Costales A and Pendás A M 1997 *Phys. Rev. B* **55** 4285
- [12] Jenkins S and Morrison I 1999 *J. Chem. Phys.* A **103** 11 041
- [13] Koch U and Popelier P L A 1995 *J. Chem. Phys.* **99** 9747
- [14] Bone R G A and Bader R F W 1996 *J. Chem. Phys.* **100** 10 892
- [15] Cremer D and Kraka E 1984 *Croatica Chem. Acta* **57** 1259
- [16] Espinosa E, Molins E and Lecomte C 1998 *Chem. Phys. Lett.* **285** 170
- [17] Jenkins S and Morrison I 2000 *Chem. Phys. Lett.* **317** 97
- [18] Abramov Yu A and Okamura F P 1997 *Acta Crystallogr. A* **53** 187